Journal of Ovonic Research Vol. 17, No. 4, July - August 2021, p. 395 - 403

Fabrication of FTO/Li_2O/ZnO/p-PSi/Al solar cell by chemical precipitation method

S. M. A. Al Hussan[a,b,*], N. A. Bakr[a], A. N. Abd[c], M. A. Khalaf[c]
[a]*Department of Physics, College of Science, University of Diyala, Diyala, Iraq*
[b]*Bilad Alrafidain University College, Diyala, Iraq*
[c]*Department of Physics, College of Science, Mustansiriyah University, Baghdad, Iraq*

In this paper, electrochemical etching of the p-type silicon wafer is used to prepare p-type porous silicon with a current density of 10 mA.cm^{-2} for 10 minutes. Zinc oxide and lithium oxide nanoparticles are prepared separately by chemical precipitation method and simple precipitation method respectively and deposited on glass substrates by drop-casting method. Moreover, the structural and optical properties of the films were analyzed by using XRD and UV-Vis. The XRD results showed that the ZnO and Li_2O films are polycrystalline with hexagonal wurtzite structure and cubic structure, and preferred orientation along (101) and (003) planes, respectively. Using Scherrer's formula, the crystallite size was measured and it was found that ZnO and Li_2O thin films have a crystallite size of 22.04 and 45.6 nm respectively. The atomic force microscope image and the distribution chart of the grains of the ZnO and Li_2O films displayed the grain sizes of~ 58.45 and 83.19 nm. The absorption coefficient spectrum of films were recorded by Ultra Violet–Visible spectrophotometer. The energy band gaps of the films calculated by Tauc's formula were ~ 4.18 and 5.5 eV. The results demonstrated that the conversion efficiency for Al/Li_2O/ZnO/p-PSi/Al, Al/Li_2O/ZnO/FTO and FTO/Li_2O/ZnO/p-PSi/Al tandem (porous silicon/FTO) solar cells were 0.313%, 0.764% and 24.6%.

(Received April 22, 2021; Accepted August 18, 2021)

Keywords: ZnO: Li_2O thin films, ECE, PSi, Tandem solar cell, efficiency

1. Introduction

Photovoltaic cells convert solar energy into direct current electricity using p-type and n-type semiconductors. Traditionally, solid-state junction devices, which are typically made of silicon, have dominated this area, drawing on semiconductor industry experience and material availability. Among various semiconductor devices used for the conversion of solar light into electrical power, the common porous silicon photovoltaic cells are the most popular. For many years, investigations have been carried out to improve the most significant parameters of these cells such as open-circuit voltage (Voc), short-circuit current (Isc), fill factor (FF), and efficiency (g). Efforts have also been made to simplify the fabrication process and reduce the cost of production. Several methods to quantization, such as quantum well and quantum dot devices, have been proposed over the last two decades such asbandgap modulation, optical absorption enhancement, and indirect-to direct bandgap formation which can be used for more efficient photo conversion processes [1]. Porous Silicon (PS) is a sponge-like material which is modeled as silicon quantum wires or dots. Canham was the first to note apparent photoluminescence (PL) at room temperature, [2] indicating that the bandgap broadening of PS compared to bulk silicon and formation of a heterojunction between PS and silicon substrate according to quantum confinement model, photoconductivity (PC) and photovoltaic (PV) properties of this material were reported [3–5]. Besides these properties, the low reflection losses and large active area for light–semiconductor interaction as results of its porous nature, absorption spectrum in the range 0.8–1.3 eV and H-passivated surface make PL a promising material for use in silicon solar cell technology [6–8]. In the last decades, several authors have reviewed PS application in mono and multi-crystalline silicon solar cells as an antireflection coating or a window layer in heterojunction cell structure [6–12]. This paper focuses on the fabrication of multilayers which consist of the first base porous

* Corresponding author: shahlamn91@yahoo.com

silicon structure and application of such structure in Si photovoltaic devices. Generally, PS multilayers can be formed by the electrochemical etching method. During the reaction, the current density and time anode are identical (10) and in the second base FTO. However, in this work, we present a new approach for the formation of the multi-layer structure by using two bases. Our results demonstrate that the application of a multi-layer could enhance the output current of photovoltaic cells.

2. Experimental work

2.1. Fabrication of porous silicon

p+ silicon wafer (5 Ω/cm^2, 500 µm), from (Bioanalyse, Turkey) with an orientation of (100) was used as a substrate. It was first washed by ultrasound bath twice with acetone and methanol. HF (45%) was then diluted at a 1:10 ratio to distilled water (DI), and the surface was engraved to eliminate any remaining particles on the Si-surface. Porous silicon was prepared by electrochemical etching of Si wafer surface. Instead of a mixture of HF (48%) and absolute ethanol, cleaned Si was put on the bottom of the Teflon cells with a ratio 1:1. A gold ring was used within 10 min as an electrode with a current density of 10 mA.cm^{-2}. After that, the porous silicon was soaked in distilled water before it driedby nitrogen gas [13], as seen in Fig.1.

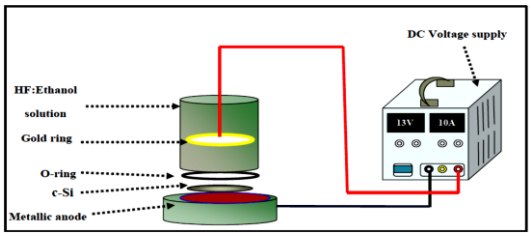

Fig. 1. Schematic diagram of the electrochemical etching.

3. Preparation of nanoparticles

3.1. ZnO nanoparticles

ZnO NPs were prepared by the chemical precipitation method. Zinc chloride ($ZnCl_2$) and sodium hydroxide (NaOH) were used as precursors and Poly (vinyl chloride) (PVC) as a stabiliser. Using a standard procedure, 13.6 g of $ZnCl_2$ (Central Drug House (P) India, 97.0%) solution was prepared in 100 ml of DI water and kept under constant stirring at 75 °C for complete dissolution, which shows transparency. Then, the desired amount (25 ml) of NaOH (1 M) and 0.5 g of PVC (Sigma Aldrich USA, 99.9%) was used during a typical transaction. At the end of the reaction, the solution was allowed to settle, and the supernatant layer was poured off and washed with double distilled water and ethyl alcohol. The washing procedure was done several times in order to remove the residual impurities present in the sample. The final white products were dried at 500°C in a hot air oven for 1 hour to obtain nanosized ZnO powder particles. The following chemical reactions show the decomposition process of the solution compound used:

$$2ZnCl_2 + 2NaOH \longrightarrow ZnO + 2\,NaCl_2 + H_2\uparrow$$

3.2. Li_2O nanoparticles

Li_2O NPs were prepared using a simple precipitation method. An amount of 0.6 g of lithium powder (MART India, 99.9%) was dissolved in 100 ml of DI water and kept under constant stirring at 80 °C for complete dissolution. Lithium intensively reacts with water, producing high flammable lithium hydroxide and hydrogen. The highly alkaline solution is colorless [14], as shown in the reaction:

$$2Li + 2H_2O \rightarrow 2LiOH + H_2\uparrow$$

Further heating decomposes lithium hydroxide (LiOH) to obtain white colour (Li_2O), according to the reaction [15]:

$$2LiOH(s) \rightarrow Li_2O(s) + H_2O\ (g)$$

4. Device Fabrication

Preparation of Multijunction Solar Cells and the conversion efficiency of porous silicon cells can be improved by the preparation of the tandem solar cell. The FTO/Li_2O/ZnO/p-PSi/Al multi-junction device structure is shown in Fig.2. The porous silicon solar cells and the FTO solar cells were used as bottom cells and top cells respectively to design tandem solar cells. The PSi cells were previously prepared in an electrochemical etching method, the FTO glass substrates were cleaned in an ultrasonic bath with deionized water, acetone and ethanol sequentially for (10 min). ZnO and Li_2O layer were then deposited upon the upper FTO and PSi substrate at (80 °C) by the drop-casting method. The two cells (PS and FTO) were mechanically stacked on top of each other. The silicon used in this work was P-type. The aluminum layer was deposited by thermal evaporation technique on the backside of PSi cells. Finally, FTO and Al electrodes were connected electrically to Keithley source by wires to perform the efficiency test.

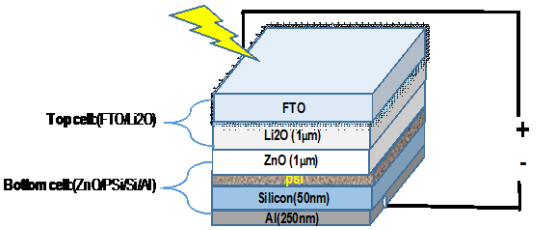

Fig. 2. Schematic of FTO/Li_2O/ZnO/p-PSi/Al device structure.

5. Characterization

The crystalline phase and crystallite size of ZnO and Li_2O thin films were characterized by using X-ray Difractometer, type Shimadzu 6000 type (Japan) utilizing CuKα radiation (λ=1.5406 Å) scan from (10° to 70°). The crystallite size is determined using the Scherrer formula using the relationship [16]:

$$D = \frac{K\,\lambda}{\beta\ Cos\ \theta} \quad (1)$$

where, (K) is constant, (λ) is the wavelength of x-ray, which is equal to 0.15406 nm, (β) is the full-width at half-maximum, and (θ) is Bragg angle. Optical absorbance for ZnO and Li_2O thin films was obtained at room temperature via (UV–VIS-NIR) spectrophotometer (type Shimadzu, UV-1800). The data of the absorbance are used to calculate the absorption coefficient by using equation[17]:

$$\alpha = \frac{(2.303 \times A)}{t} \quad (2)$$

where, α is the absorption coefficient, A is the absorbance and t**:** is the thickness.

The energy gap (E_g) is calculated using (Tauc equation)[18]:

$$\alpha h\nu = A(h\nu - E_g)^n \quad (3)$$

where, (α) is the coefficient of absorption, (hν) is the energy of photon, (A) is a constant that does not rely upon the energy of photon, (Eg) is the optical bandgap and (n) possesses four numeric values (1/2) for allowed direct, (2) for allowed indirect, (3) for forbidden direct and (3/2) for forbidden indirect optical shifts.

The characteristics of the Current–Voltage (I-V) of FTO/ZnO/Li_2O/PSi/p-Si/Al tandem solar cells were tested using a Keithley 2400 source meter under light source (10 mW/m^2). Depending upon the (I–V) curve, the fill factor (FF) was computed by the following equation [19]:

$$FF(\%) = \frac{J_{max}V_{max}}{J_{sc}V_{oc}} = \frac{P_{max}}{J_{sc}V_{oc}} \times 100\% \quad (4)$$

where: P_{max}: The maximum power, J_{sc}: The density of the short-circuit photocurrent, Voc: The open-circuit photo voltage.

The efficiency (η) of photoelectric conversion was computed by this formula [20]: where P_{in} is the incident power.

$$FF(\%) = \frac{J_{max}V_{max}}{J_{sc}V_{oc}} = \frac{P_{max}}{J_{sc}V_{oc}} \times 100\% \quad (5)$$

6. Results and Discussion

6.1 Structural analysis

The patterns of X-ray diffraction for the crystalline nature of the synthesized ZnO and Li_2O thin films in Figure 3 are shown. Figure 3(a) presents the XRD patterns of (ZnO) thin films. From Figure 3(a), it should be noted that the patterns have peaks around diffraction 2θ~ 31.723, 34.378, 36.199, 47.493, 56.539, 62.798, 67.897 and 68.991, referred to (100), (002), (101), (102), (110), (103), (112) and (201) favorite directions respectively, which agree with the JCPDS card no. 00-036-1451, and also with other reports [21]. The favorite direction is presented in Table (**1**). The diffraction peaks of the prepared thin film show a hexagonal wurtzite structure. Accordingly, the XRD results revealed that the film obtained in this study consisted of a pure (ZnO) phase without any secondary phases. Figure 3(b) displays the XRD patterns of Li_2O thin films prepared from pure Lithium. From the figure, it can be noted that the patterns exhibit diffraction peaks around 2θ~ 30.319, 33.513, 36.023 and 63.020 referring to (101), (003), (012) and (202) favorite directions respectively. The diffraction peaks of prepared thin film exhibit cubic structure, which is in agreement with the JCPDS card no. 01-074-6256. Other peaks are due to the phase formation of non-oxidized lithium and lithium oxide represented by Li, Li_2O_2, and LiO_2 which are assigned in the figure by the symbols (*,• and ♦) respectively. These results are in agreement with previous reports [21-23].

As is well known, Li's reactivity with oxygen is extremely high and in theory different Li-O compounds can arise based on the oxidative status and complexes of dioxygen together with Li-ions. [23]. The lattice parameters for ZnO were found to be equal to a = b = 0.3253 nm, and c = 0.5217 nm. Both values are consistent with the theoretical values (a = 0.3249 nm and c = 0.5206 nm) and with other studies, respectively. [24, 25]. On the other hand, the lattice parameters for Li_2O were found to be a=b=c= 4.627 nm, which is in agreement with theoretical value a=4.610 nm and other reports [26]. For the ZnO and Li_2O films, the crystallite size is determined using the Scherrer formula.

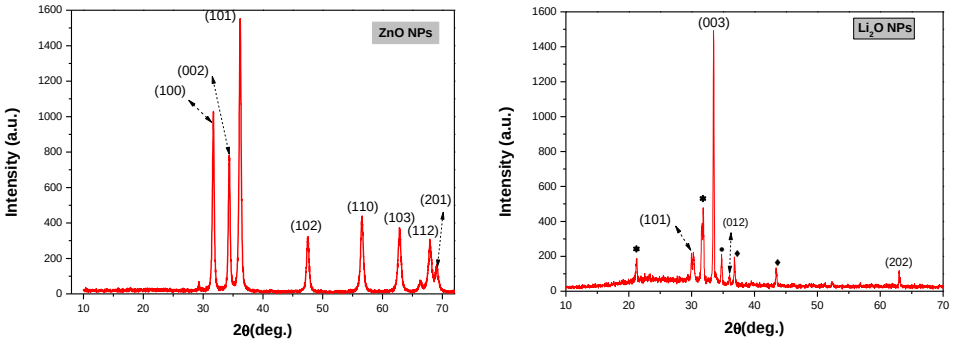

Fig. 3. The XRD patterns of (a): ZnO NPs thin films, (b): Li_2O NPs thin film.

Table 1. Structural parameters of (ZnO, Li_2O) thin films.

Parameters	**Zinc oxide (ZnO)**		**Lithium oxide (Li_2O)**	
2Θ (deg)	36.199		33.513	
hkl	(101)		(003)	
d (Å)	2.479		2.671	
(FWHM) (rad)	0.0066		0.0031	
(D) (nm)	22.04		45.6	
Lattice Constants (nm)	a=b	0.3253	a=b=c	4.627
	c	0.5217		

6.2. Atomic Force Microscope (AFM) Results

The surface morphology of the deposited ZnO and Li_2O thin films is carried out using AFM which gives the surface grain size directly. Fig.4 illustrates the morphology of the deposited thin films showing large numbers of grain; these crystallite clusters are the result of crystallite coalescence. They have a semi-ball form with a high density of distribution, homogenous grains and aligned vertically. Using special software (4.62 imager), the grain size, average roughness and root mean square of the films are estimated and listed in Table (**2**). From the table, the grain size for ZnO and Li_2O thin films are 58.45 nm and 83.19 nm respectively, which is in agreement with the result Aboud et al. [27]. 3D images prove that the grains are uniformly distributed within the scanning area (2000 x 2000 nm) with individual columnar grains extending upwards. This surface characteristic is important for solar cells and photodetector (PD).

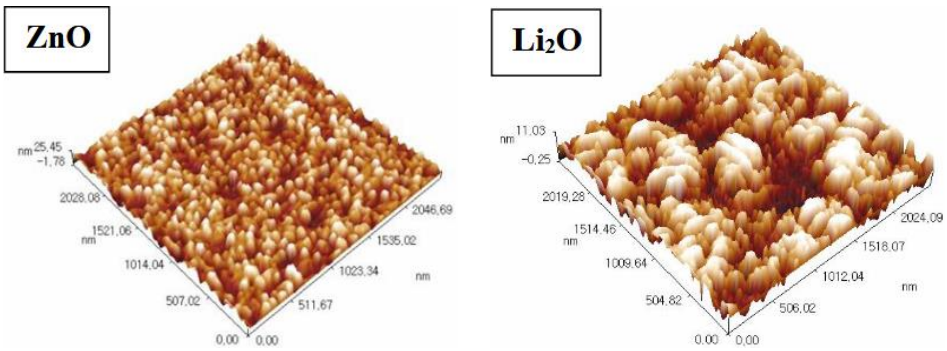

Fig. 4. 3-D AFM images of ZnO and Li_2O thin films.

Table 2. Structural parameters of (ZnO, Li_2O) thin films.

Thin films	Surface roughness average (nm)	RMS (nm)	Average grain size (nm)
ZnO	4.34	5.32	58.45
Li_2O	2.59	3.03	83.19

Granularity accumulation distribution charts of ZnO and Li_2O thin films are shown in Fig. 5. It is possible to define the particle size distribution from the diagram. The roughness peak heights were measured to be between 2 and 9 nm, and the form indicates the thin film total homogeneity on the glass.

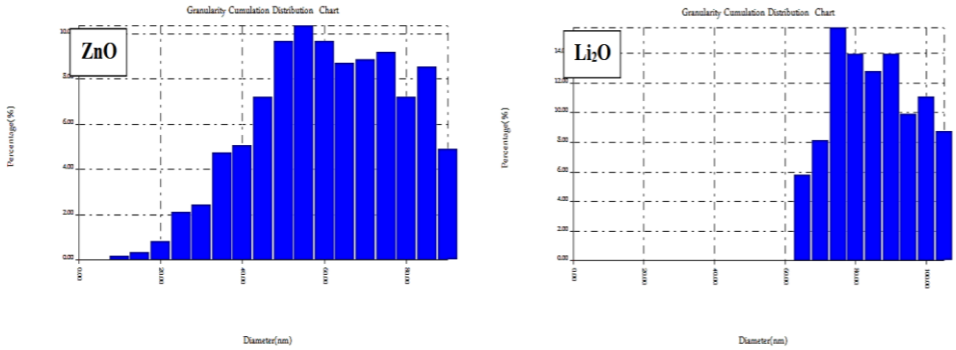

Fig. 5. Granularity accumulation distribution charts of ZnO and Li_2O thin films.

6.3 Absorption Coefficient (α)

The data of the absorbance are used to calculate the absorption coefficient by using equation(2). Fig. 6 shows the optical absorption coefficient as a function of incident photon energy for ZnO and Li_2O films. It can be seen that the thin films have a value of absorption coefficient $\alpha > (10^4)$ cm^{-1} which indicates the increase of the probability of the occurrence of direct transitions. It has been noticed that the prepared ZnO and Li_2O thin films have a high absorption coefficient between $(1.6 \text{ and } 1.45)x10^5$ cm^{-1} respectively, in the visible range and the near-IR spectral range which is in agreement with other reports [28].

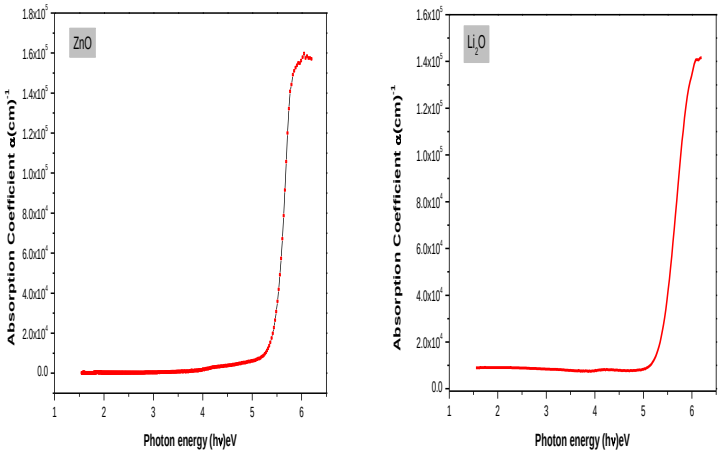

Fig. 6. The absorption coefficient of ZnO and Li_2O thin films as a function of photon energy.

6.4 Optical Energy Band Gap (E_g)

The optical energy gap for these films was measured using the absorption coefficient values. Fig.7 shows the plot of $(\alpha h\nu)^2$ vs. photon energy ($h\nu$). The energy gap is calculated using (Tauc equation) by assuming the allowed direct transition (r=1/2) between valance and conduction bands according to equation(3).

The energy gap values depend in general on the film's crystal structure and the arrangement and distribution of atoms in the crystal lattice. The extrapolation of the straight line fitting to $(\alpha h\nu)^2 = 0$ gives the value of the direct band gap, and this could be seen in Fig.7. It was found that the value of energy gap for (ZnO) film is 4.18 eV, which is a very high value compared to that of ZnO, This may be attributed to the creation of clusters combined with a low annealing temperature[29]. The physical properties of semiconducting materials change as their dimensions shrink to the nanometer scale, a phenomenon known as "quantum size effects."For example, quantum confinement increases the band gap energy of ZnO [30], while the value of the energy gap for (Li_2O) film is (5.5 eV). Since low-energy electrons in solids have very short mean free paths (as little as a few atomic planes) [31], the fundamental valence-to-conduction band gap is large, according to optical absorption measurements on single-crystal and sintered polycrystalline Li_2O.

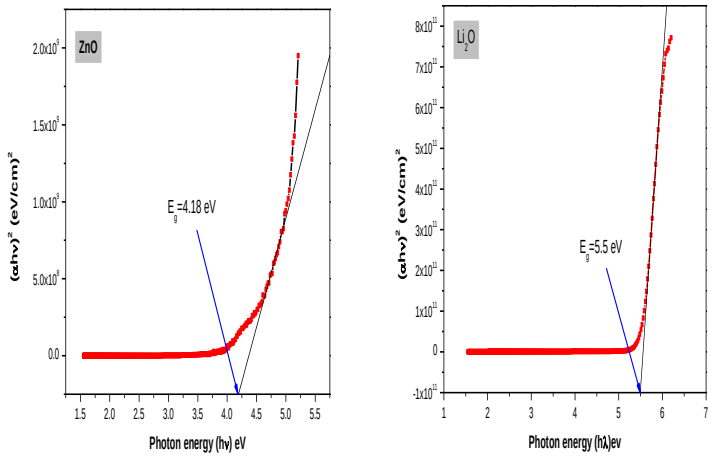

Fig. 7. Tauc's plot of ZnO and Li_2O thin films.

6.5. (J-V)characterization

The measured open-circuit voltage (Voc), short-circuit current density (Jsc), fill factor (FF %) and efficiency (η) were calculated. Fig.8 shows the (J-V) curve of the solar cell (SC) for FTO/Li_2O/ZnO/p-PSi/Al tandem device. From the figure, the efficiency for the device (24%), is higher compared to Li_2O/ZnO/p-PSi and Li_2O/ZnO/FTO, due to the absorption of photons with different wavelengths. Because of each material's p-n junction, which reduces the probability of recombination due to the length of lifetime, it is longer than in heterojunction solar cells, and in turn, will produce an electric current in response to different wavelengths of light. For the absorbance of a wider spectrum of wavelengths, several semiconducting materials are used. Also, by covering a greater portion of the solar spectrum and obtaining a higher open-circuit voltage (V_{OC}), the cell's efficiency in converting sunlight to electrical energy is improved[32].

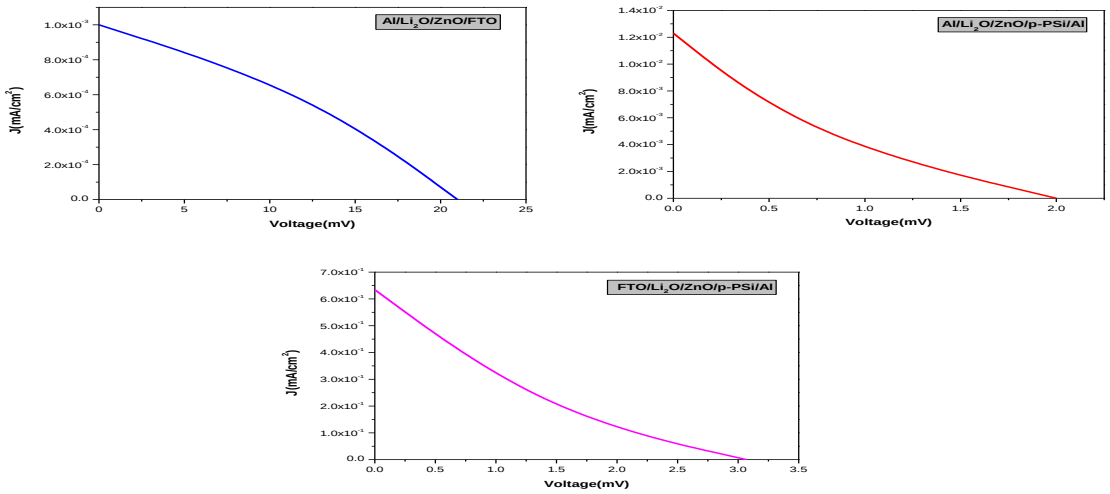

Fig. 8. (J-V) curve of solar cell (SC) for Al/ZnO/Li_2O/ p-PSi/Al, Al/ZnO/Li_2O/FTO. hetetrojunction and FTO/ZnO/Li_2O/ p-PSi/Al tandem devices.

Table 3. (J-V) measurements of solar cells (SC) for hetetrojunction and multijunction.

Solar cells	J_m (mA/cm^2)$\times 10^{-2}$	V_m (mV)	J_{SC} (mA/cm^2)$\times 10^{-2}$	V_{OC} (mV)	F.F%	η%
Al/Li_2O/ZnO/p-PSi/Al	0.44	0.7	1.23	2	12.70	0.313
Al/Li_2O/ZnO/FTO	0.061	12.5	0.1	21	35.71	0.764
FTO/Li_2O/ZnO/p-PSi/Al	17	1.40	63.43	3.07	12.63	24.6

7. Conclusion

In this study, ZnO and Li_2O thin films were successfully prepared and deposited on glass substrates by drop-casting method. XRD patterns of ZnO and Li_2O thin films show that the films are polycrystalline with hexagonal wurtzite structure and cubic structure, respectively. The major peak characteristics are allocated to planes (101) and (003), respectively. XRD analysis of Li_2O thin films shows the presence of other diffraction peaks which were attributed to Li, Li_2O_2, and LiO_2 phases. Porous silicon has been successfully prepared of the silicon wafer (p+) by electrochemical etching. ZnO and Li_2O films have been successfully deposited on porous silicon via the drop-casting process. According to the absorption spectra, the ZnO and Li_2O films are characterized by a wide range of absorption, which extends from the visible region to the near-infrared region and is therefore used as a window layer and absorbent layer respectively, in the solar cells. The fabrication of a new kind of solar cell, called a tandem device, increased the performance of porous silicon cells. The tandem device recorded higher efficiency compared to porous silicon and FTO devices.

References

[1] Y. Hamakawa, Thin-Film Solar Cells, , 39 (2004).
[2] L. T. Canham, Appl. Phys. Lett. **57**, 1046 (1990).
[3] N. Koshida, H. Koyama, Proc. Mater. Res. Soc. Symp. **256**, 219 (1992)
[4] G. Smestad, M. Kunst, C. Vial, Sol. Energy Mater. Sol. Cells **26**, 277 (1992).
[5] F. Yan, X. Bao, T. Gao, Solid State Commun. **91**, 341 (1994).
[6] V. Pacebutas, K. Grigoras, A. Krotkus, Phys. Scr. **T69**, 255 (1997).

[7] P. Vitanov, M. Kamenova, N. Tyutyundzhiev, M. Delibsheva, E. Goranova, M. Peneva, Thin Solid Films **297**, 299 (1997).
[8] P. Vitanov, M. Delibasheva, E. Goranova, M. Peneva, Sol. Energy Mater. Sol. Cells **61**, 213 000).
[9] P. Vitanov, M. Kamenova, N. Tyutyundzhiev, V. Gantcheva, Proceeding of Solar World Congress, Harare, (1995).
[10] Z. N. Adamin, A. P. Hakhoyan, V. M. Aroutiounian, R. S. Barseghian, K. Touryan, Sol. Energy Mater. Sol. Cells **64**, 347 (2000).
[11] K. Drabczyk, P. Panek, M. Lipinski, Sol. Energy Mater. Sol. Cells **76**, 545 (2003).
[12] L. Kore, G. Bosman, Sol. Energy Mater. Sol. Cells **57**, 31 (1999).
[13] R. Ramadan, Miguel Manso-Silván, Raúl J. Martín-Palma, Journal of Materials Science **55**(13), 1 (2020).
[14] Mark S. Ortman, Edwin M. Larsen, Preparation, Journal of the American Ceramic Society-Ortman and Larsen) **66**(9), (1983).
[15] L. N. Dinh, W. McLean, M. A. Schildbach, J. D. LeMay, W. J. Siekhaus, M. Balooch, Journal of Nuclear Materials **317**, 175 (2003).
[16] Ahmed N. Abd, Shahlaa M. Abd Al Hussan, Duha M.A. Latif, Plant Archives **20**(1), 2469 (2020).
[17] Nibras Abdul-Ameer Aboud, Wafaa M. S. Alkayat, Dhia H. Hussain, Sys Rev Pharm **11**(6), 1188 (2020).
[18] Shahlaa M. Abd Al-hussan, Effect of Substrate Temperature on Structural and Optical Properties of Cu_2ZnSnS_4(CZTS) Films Prepared by Chemical Spray Pyrolysis Method, A Thesis Submitted to the College of Science University of Diyala, Master In Physics, (2015).
[19] Nabeel A. Bakr, Abdul Rahman K. Ali, Shaimaa M. Jassim, Journal of Garmian University Conference Paper, (2017).
[20] H. Föll, M. Christophersen, J. Carstensen, G. Hasse, Mater. Sci. Eng. R **39**(4), 93 (2002).
[21] Mahendra Kumar Trivedi, Rama Mohan Tallapragada, Alice Branton, Dahryn Trivedi, Gopa Nayak, Omprakash Latiya, Snehasis Jana, J Adv. Chem. Eng. **5**(4), (2015).
[22] Kah Chun Lau, Dantong Qiu, Xiangyi Luo, Jeffrey Greeley, Larry A. Curtiss, Jun Lu, Khalil Amine, Energies **8**, 529 (2015).
[23] Xinmin Zhang, Limin Guo, Linfeng Gan, Yantao Zhang, Jing Wang, Lee Johnson, Peter G. Bruce, Zhangquan Peng, J. Phys. Chem. Lett., 1 (2017).
[24] L. Fadillah, B. Soegijono, S. Budiawanti, I. Mudzakir, AIP Conference Proceedings **1862**, 030053 (2017).
[25] Zahra Monsef Khoshhesab, Mohammad Sarfaraz, Mohsen Asadi Asadabadm, Metal-Organic, and Nano-Metal Chemistry **41**, 814 (2011).
[26] W. I. F. David, M. O. Jones, D. H. Gregory, C. M. Jewell, S. R. Johnson, A. Walton, P. P. Edwards, A. Edwards, Journal of the American Chemical Society **129**(6), 1594 (2007).
[27] J. D. Wolfe, N. L. Thomas, US Patent **6078**(6), 25 (2000).
[28] C. Zhang, W. Luan, Y. Yin, Energy Proc. **105**, 793 (2017).
[29] Rezq Naji Aljawfi, Moh. Jane Alam, F. Rahman, Shabbir Ahmad, Aga Shaheec, Shalendra Kumar, Arabian Journal of Chemistry **S1878-5352**(18), 30087-X (2018).
[30] X. Wang, Y. Ding, C. J. Summers, Z. L.Wang, Journal of Physical Chemistry B **108**(26), 8773 (2004).
[31] Lizhong Liu, Victor E. Henrich, W. P. Ellis, I. Shindo, Physical review B **54**(3), (1996).
[32] W. I. F. David, M. O. Jones, D. H. Gregory, C. M. Jewell, S. R. Johnson, A. Walton, A. Edwards, P. P. Edwards, Journal of the American Chemical Society **129**(6), 1594 (2007).